PROCEEDINGS, 49th Workshop on Geothermal Reservoir Engineering
Stanford University, Stanford, California, February 12-14, 2024
SGP-TR-227

Experimental Study of the Mineral Precipitation Dynamics During Geothermal Reinjection

Anna Kottsova[1,2], Xiang-Zhao Kong[2], Pacelli L.J. Zitha[2], David F. Bruhn[2], Martin O.Saar[1], Maren Brehme[1]

[1]ETH Zurich, Geothermal Energy and Geofluids, Department of Earth Sciences, Zurich, Switzerland

[2]Delft University of Technology, Department of Geosciences and Engineering, Delft, the Netherlands

akottsova@ethz.ch

Keywords: mineral precipitation, chemical clogging, flow-through experiments, geothermal reinjection

ABSTRACT

The efficiency of geothermal energy extraction strongly depends on the productivity and injectivity of the wells. These are governed by porosity, permeability, fluid properties and flow conditions in the reservoir, wellbores, and surface facilities. Permeability and fluid conditions can be altered by various processes, such as mineral precipitation, fines production and migration, thermal fracturing, etc. Understanding the underlying mechanisms of such processes is essential for the optimal selection of operating conditions that ensure efficient reservoir utilization. In this work, we study the dynamics of mineral precipitation triggered by the mixing of two incompatible fluids in the pore space. For that, we perform core-flooding experiments and monitor fluid pressures along the sandstone specimen and simultaneously visualize the precipitation pattern by X-ray micro-CT scanning at a spatial resolution of 12 um. The experimental parameters (such as ionic concentrations and injection flow rates) are screened with the help of a numerical model, which is developed to further delineate reaction kinetics and reactive transport of the chemical species in the pore space. Our study provides insights into the mechanisms of chemical clogging and a reference for further research on reactive transport involving mineral precipitation. Understanding the time evolution of precipitation, its location in the pore space and quantifying the effect on permeability remain a challenge but are of utmost importance for optimal planning of the operational schemes. This study has received funding from the European Union as part of the EASYGO-ITN.

1. INTRODUCTION

One of the key parameters of the geothermal reservoir performance is the reservoir injectivity, generally represented by the injectivity index, which is a measure of fluid intake at a given wellhead pressure (Zarrouk et al., 2019). Injectivity is governed by various properties of reservoirs, including porosity, permeability and fluid properties. During geothermal operation, these parameters can be altered by different processes, which can be essentially divided into two groups – injectivity decline and injectivity enhancement (Luo et al., 2023). While injectivity enhancement can be a desirable process, injectivity decline is an unwanted yet common consequence of geothermal reinjection. The decline of injectivity is typically caused by clogging due to physical, chemical and biological processes. In this study, we focus on the chemical precipitation, which has been shown to have a strong impact on the reservoir performance (e.g., Brehme et al., 2018). Mineral precipitation can lead to a reduction of the injectivity index up to 20% (Luo et al., 2023). Understanding the underlying mechanisms and the evolution of precipitation is therefore essential for the optimal selection of operating conditions.

While commonly reinjection of the produced geothermal fluid is applied, in some cases co-injection of another fluid can be used, e.g., to compensate for the pressure loss in the vapor-dominated systems (Majer et al., 2007, Stark et al., 2005). In addition, depending on the operating conditions, fluid composition might also change in the surface facilities due to scaling during heat extraction, oxidation caused by poor insulation, etc. In this work, we investigate precipitation processes triggered by the mixing of two incompatible fluids in the pore space.

Up until now, experimental visualization of the precipitation front propagation has remained a challenge. There have been studies, focused on recreating the mineral precipitation by mixing incompatible fluids. Bray et al. (2016) visualized the front propagation of precipitation with Magnetic Resonance Imaging (MRI), providing insights into front evolution, yet not at the pore-scale resolution. Orywall et al. (2017) studied barite precipitation under elevated pressure and temperature conditions and showed the location of barite precipitates in the pore space with post-experimental Computed Tomography (CT) imaging. However, their methodology involved injecting slightly supersaturated barite solution and not direct mixing of incompatible fluids in the pore space.

In this study, we show the experimental results of the flow-through experiments on co-injection of incompatible fluids into a sandstone core sample, demonstrating the effect of direct mixing of two fluids and precipitation reaction in the pore space. Our experiments are accompanied by 12-um micro-CT scanning to gain insights into mineral precipitation localization. These experiments not only enhance our understanding of the chemical clogging process but also bring us closer to replicating real-case scenarios. In addition, the experimental work is combined with a 2D numerical model of the reactive transport to delineate reaction kinetics and select optimal experimental parameters.

2. METHODOLOGY

2.1 Rock and Fluids Characterization

The experiments aim to induce mineral precipitation in porous media through fluid-fluid mixing. To minimize the influence of fluid-rock interactions, we use Berea sandstone as a representative porous medium. X-ray diffraction (XRD) analysis shows more than 90% of SiO_2 in this Berea sandstone, thus it is considered inert (negligible chemical reactions between the injected fluids and the formation minerals) during the flow-through experiments. CT images show homogeneous pore space throughout a sub-cored specimen of a length of 15 cm and a diameter of 2.54 cm. The initial porosity of the specimen was measured to be 20%, giving a pore volume (PV) of ca. 15 cm^3. Its initial bulk permeability was measured to be 30 mD.

Given its low solubility, barite is chosen to be the precipitated mineral induced by the following chemical reaction:

$$BaCl_2 + Na_2SO_4 \rightarrow BaSO_4\downarrow + 2\,NaCl \quad (1)$$

The associated reaction kinetics are examined using the Reaktoro chemical software (Leal, 2015), prior to the physical experiments. Based on the preliminary chemical modeling, solutions of $BaCl_2$ and Na_2SO_4 with a concentration of 10 mM are chosen for the experiments, which would avoid immediate blockage around the injection inlet and allow propagation of the precipitation front throughout the specimen. Additionally, higher density of barite in comparison to sandstone enables effective monitoring of its precipitation reaction through micro-CT scanning.

2.2 Experimental Setup

Figure 1 shows the setup of the experimental approach, where the sandstone core sample is encased in an X-ray transparent core holder to allow in-situ micro-CT scanning. The core holder is self-designed and fabricated with 3D-printing technology. Individual core holder design allows high flexibility in choosing diameter and length of a sample as well as placement of injection points and pressure sensors. Epoxy resin is applied to create an impermeable layer around the specimen to force fluid flow in the specimen.

The permeability evolution is indirectly monitored with a 10-bar range pressure sensor at the inlet and two 3-bar range differential pressure sensors along the specimen. The accuracy of all sensors used is 0.05% full scale (FS). The inlet pressure sensor yields the overall permeability change, and the installation of differential pressure sensors divides the specimen into three equal intervals, namely S1 (from the main injection point to the monitoring point of the dP1 sensor), S2 (between the monitoring points of dP1 and dP2 sensors), and S3 (from the monitoring point of dP2 sensor to the outlet). This allows monitoring of individual permeability change in different sections along the sample, calculated with the help of Darcy's law.

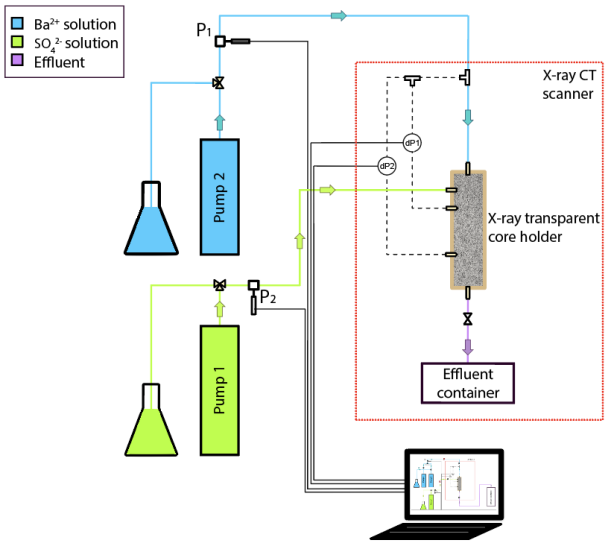

Figure 1: Schematic of the core flooding setup. Experimental design includes two fluid injection ports, pressure (P) and differential pressure (dP) sensors for monitoring permeability change.

To force fluid mixing only in the rock sample and avoid immediate reaction in the tubing, two fluids were simultaneously injected from two injection points. The core holder is equipped with two injection points: main injection, from the top of the core holder and side injection of the secondary fluid (Figure 1). Such design replicates the fluid mixing in the reservoir and allows flexible selections of the pore velocities ratio between the two fluids to realize different field scenarios.

The specimen is initially saturated and equilibrated with the Na_2SO_4 solution through the main injection point, then initial bulk permeability is measured at equilibrium Darcy flow of the same solution. The precipitation of barite is then induced by co-injection of the $BaCl_2$ solution from the side injection point. Effluents, each of ½ PV (i.e. 7.5 cm^3), are collected at the outlet (at 1 atm) for the post-experimental analysis.

Flow velocities are chosen according to the fluid velocity profile along the fluid path in a radial flow using the following equations:

$$v_w = \frac{Q_{inj}}{2\pi r_w h\, \phi} \quad (1)$$

$$v(r) = \frac{r_w v_w}{r} \quad (2)$$

where $Q_{inj}, h, \phi, v(r), r, v_w, r_w$ are injection rate, reservoir thickness, porosity, fluid velocity, distance from the wellbore, fluid velocity at the injection well, and wellbore radius, respectively. The resulting radial velocity profile is shown in Figure 2, along with selected pairs of flow rates for two stages during the experiments. The detailed experimental parameters are documented in Table 1. The main flow of the Na_2SO_4 solution represents the reservoir background flow with a small cross-sectional velocity, while the side injection represents the flow of the $BaCl_2$ solution from the injection well, coming at a relatively high cross-sectional velocity. The injection of fluid is maintained by two pulsation-free pumps during the experiments.

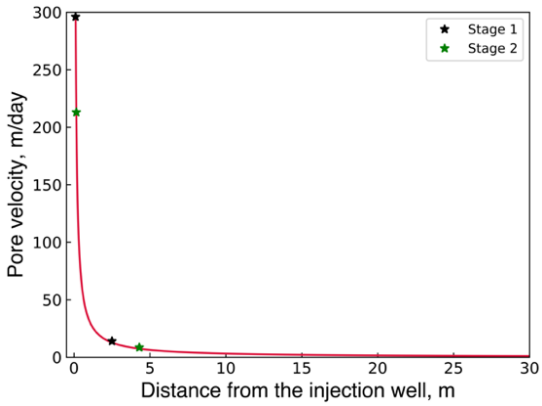

Figure 2: Pore velocity profile along the fluid flow path (radial flow).

Table 1: Experimental parameters

	Stage 1 flow rate, mL/min	Stage 2 flow rate, mL/min	Injected fluid
Main injection	0.6	1.02	Na_2SO_4, 10 mM solution
Side injection	0.09	0.18	$BaCl_2$, 10 mM solution

3. RESULTS AND DISCUSSION

3.1 Pressure Measurements

The presented figures illustrate the recorded pressure measurements (P1, P2) from the injection point (Figure 3a) and readings from the differential pressure sensors (dP1, dP2) along the specimen (Figure 3b). Pressure drops in the three sections of the core, defined earlier, are indicated by ΔP1, ΔP2, and ΔP3 in Figure 3c. To facilitate a meaningful comparison of precipitation effects on pressure, and consequently permeability, at various injection flow rates, the ΔP/Q value is used, where Q is the sum of the two volumetric flow rates. Overall, the pressure graphs can be divided into four distinct zones, represented by different color shading, each reflecting a different impact of precipitation reaction on the specimen permeability. In the following, we mainly focus on Figure 3c.

Zone 1 corresponds to the co-injection at the low flow rates of 0.6 and 0.09 mL/min. In the beginning a notable increase in all ΔP/Q values is seen, caused by the re-establishment of fluid flow regime in the specimen. The sharp increases in ΔP1/Q and ΔP2/Q are followed by an asymptotical decrease, which is part of the re-establishment of fluid flow. While ΔP3/Q shows a much higher initial increase in comparison to ΔP1/Q and ΔP2/Q, this increase is believed to be due to the deposition of fine particles from the upstream in Section S3. This deposition leads to minor permeability impairment due to clogging of pore space, which is later restored as fine particles are flooded out of the specimen at the end of Zone 1. A small subsequent increase of the pressure drop across sections S1 and S2 is seen after injection of 2 and 5 PV, respectively, indicating the growth of the precipitation front. The stepping change in Zone 1 was caused by an unexpected short stop of the main injection pump, which introduced an irreversible steep increase in ΔP2/Q, which might be partially responsible for the thickening of precipitation in Section S2 (Figure 4a).

After an injection of 15 PV solution, the flow rates are increased to 1.02 and 0.18 mL/min, respectively, resulting in an immediate decrease in ΔP/Q. All three sections show slow increase in ΔP/Q in Zone 2, suggesting clogging of the pore space due to precipitation, as shown in Figure 3c. Overall, the increase in ΔP/Q is rather mild because the deposition of the precipitated barite is parallel to the main flow (Figure 4a). Despite the similar length of all three intervals, Section S2 displays an overall higher ΔP /Q value, compared to the other sections. This could be the effect of the amount of precipitated barite, which is limited in Section 1 due to the position of the injection point and has not yet reached the Section 3 in sufficient concentration.

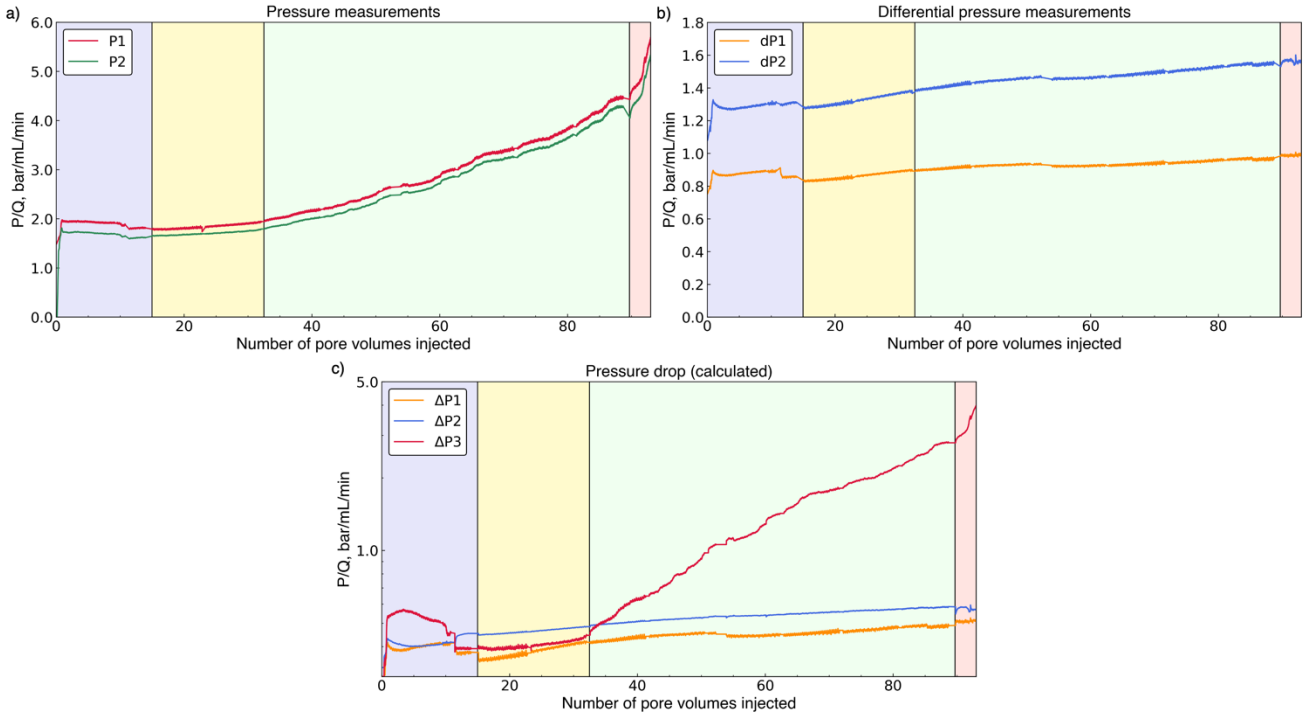

Figure 3: Pressure measurements during the flow-through experiment: a) pressure measured from sensors P1 and P2; b) differential pressure measured from sensors dP1 and dP2; c) calculated pressure drop ΔP for three specimen sections.

Zone 3 is marked by a profound increase in ΔP3/Q after an injection of 33 PVs. We interpret such behavior as the intensifying precipitation at the outlet region, as further shown in Figure 4a. The core holder is equipped with end caps of fluid distribution network. These end caps offer large space for better mixing of Ba^{2+} and SO_4^{2-} ions and subsequent precipitation and deposition. Once both Ba^{2+} ions and SO_4^{2-} ions reach the outlet in sufficient concentration, precipitation is accelerated due to better mixing, resulting in blockage of the outlet and substantial rise of ΔP3/Q (Figure 3c).

The last zone is characterized by almost no changes in ΔP1/Q and ΔP2/Q, but a rapid and continuous increase in ΔP3/Q. This indicates further blockage of the end cap at the outlet end or the outlet tubing.

After the termination of the experiment, the bulk permeability of the specimen is measured again to assess the overall effect of clogging. The bulk permeability shows a significant reduction from 30 to 8 mD, indicating an approximately 70% permeability impairment, though mainly attributed to the blockage at the core outlet. Nevertheless, permeability calculations from differential pressure measurements revealed that the top (S1) and middle (S2) sections of the core experienced a comparatively less severe clogging impact, with reductions of 10% and 25% in permeability, respectively. This is still, however, a substantial decrease in permeability that could affect reservoir performance in terms of geothermal reservoir utilization.

3.2 CT Imaging Data

Figure 4 presents two-dimensional (2D) slices of the precipitation pattern. The higher density of barite, compared to the constituent minerals in Berea sandstone, allows a clear imaging of the precipitation pattern. For a more comprehensive understanding of the clogging process, we provide the images of orthogonal 2D slices in Figure 4b.

The precipitation pattern is characterized by a close circular curtain shape from the side injection point to the end of the sample. This precipitation pattern is mainly governed by the orthogonal flow velocities from two injection points. In this experiment, we do not investigate the effect of the ratio of injection volumetric rates in detail. We performed 2D reactive transport modeling prior to the experiments for experimental parameters screening, resulting in the selection of flow rates (Table 1). While we do not discuss the results of numerical simulations in detail within this paper, the observed precipitation pattern largely resembles the precipitation pattern predicted by our numerical model, except for the outlet end. The fluid distribution end cap certainly plays a role on the observed precipitation pattern close to the outlet, as the end cap tends to direct fluids towards the flow path of least resistance (Figure 4a). It is expected that the curtain displays the mixing front between the main flow and side flow. Due to the rapid kinetic rate for barite precipitation reaction and low solubility of barite in water (Zhen-Wu et al., 2016), the precipitation of barite should predominantly occur at the solution-solution interface. Figure 4b suggests the mixing front thickness is limited to about 2-4 mm, showing that due to the growth of the precipitation curtain, two fluids are becoming more and more separate and bypass each other, as inferred from the pressure data.

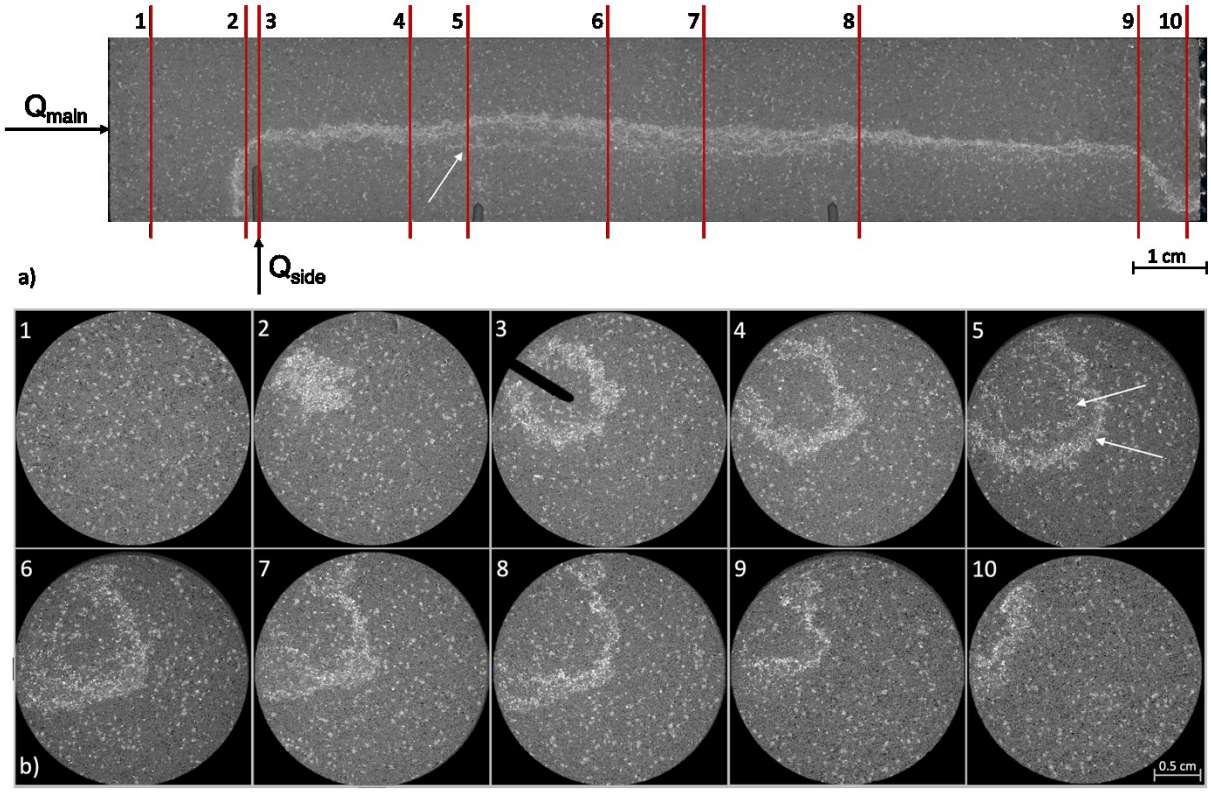

Figure 4: Micro-CT imaging data after the flow-through experiment: a) 2D profile along the core length; b) multiple XY slices of the core, numbered according to a).

Slice 3 in Figure 4b shows the side injection point of the $BaCl_2$ solution. Slice 2 presents an upward propagation of the injected $BaCl_2$ solution, where a shelter hut is formed above the injection point. Slices 5-8 showcase two layers of curtain of barite precipitation (indicated with two white arrows in Slice 5). This is most probably the result of the flow rate increase after an injection of 15 PVs. Due to this increase, the side injection has become slightly stronger in comparison to the main injection, causing a shift of the curtain towards the main flow. Figure 4a suggests that this shifting only appears at a certain distance from the injection point (indicated by an arrow). This infers that a well-established front has been formed in Section S1 during the injection of the first 15 PVs of solutions. The shifting of the precipitation front (as shown in Slice 5) indicates that in this region the precipitation boundary is still permeable and allows transport of fluids across it. As the precipitation continues and the curtain is thickening, it is becoming less permeable, leading to incompatible fluids mixing mainly at the outlet end. The blockage of the outlet end cap is clearly illustrated in Figure 4a, an independent support for the observed rapid pressure increase in Figure 3.

Overall, our CT images are in good agreement with the pressure observations and provide valuable insights into the underlying processes of precipitation dynamics. We demonstrate that mineral precipitation reaction caused by the mixing of incompatible fluids occurs mostly at the boundary between these fluids.

4. CONCLUSIONS AND OUTLOOK

Our study of barite precipitation in Berea sandstone has provided preliminary understanding of mineral precipitation dynamics and its influence on rock permeability. The pressure measurements demonstrate distinct zones representing the evolving effects of precipitation at different stages of the experiment. The analysis of pressure measurements aligns well with the CT scans of the precipitation pattern, revealing a well-defined precipitation front. Such correlation between CT data and pressure measurements reinforces the reliability of this analysis and underlines the value of high-resolution imaging techniques. The observed curtain shape of the precipitation front is governed by flow ratio between the two injected solutions. The rapid kinetics rate of barite precipitation facilitates thin reaction front, which eventually forms an impermeable boundary and restricts solution-solution contact across the boundary.

We observe that the impact of chemical clogging on the rock permeability is quite substantial, reaching 25% reduction of the bulk permeability, even though the precipitation front is parallel to the main flow. This brings up the necessity to continue investigating this effect, its potential impact on the geothermal reservoirs and possible mitigation pathways.

In future flow-through experiments, we are planning to study the effects of flow rate on the precipitation front. Further experiments will be accompanied by in-situ monitoring using the micro-CT scanner, to provide valuable insights into the dynamic evolution and propagation of the precipitation front. Future studies will also focus on restoring permeability, using both experiments and numerical

methods. We will explore ways to mitigate permeability impairment. We will further develop our numerical model to study the effect of different flow rates on the precipitation front and provide up-scale numerical solutions to the field scale applications.

AKCNOWLEDGEMENTS

The authors thank Nils Knornschild for designing and manufacturing the core-flooding setup components, as well as supervising the setup assembling process, crucial to this study. This project has received funding from the European Union's Horizon 2020 research and innovation programme under the Marie Skłodowska-Curie grant agreement No 956965. The authors also highly appreciate the support by Energi Simulation.

REFERENCES

Bray, J. M., Lauchnor, E. G., Redden, G. D., Gerlach, R., Fujita, Y., Codd, S. L., & Seymour, J. D. (2017). Impact of mineral precipitation on flow and mixing in porous media determined by microcomputed tomography and MRI. *Environmental Science & Technology*, 51(3), 1562–1569. doi:10.1021/acs.est.6b02999

Brehme, M., Regenspurg, S., Leary, P., Bulut, F., Milsch, H., Petrauskas, S., … Blöcher, G. (2018). Injection-triggered occlusion of flow pathways in geothermal operations. *Geofluids*, 2018, 1–14. doi:10.1155/2018/4694829

Leal, A.M.M. (2015). Reaktoro: An open-source unified framework for modeling chemically reactive systems. https://reaktoro.org

Luo, W., Kottsova, A., Vardon, P. J., Dieudonné, A. C., & Brehme, M. (2023). Mechanisms causing injectivity decline and enhancement in geothermal projects. *Renewable and Sustainable Energy Reviews*, 185(113623), 113623. doi:10.1016/j.rser.2023.113623

Majer, E. L., & Peterson, J. E. (2007). The impact of injection on seismicity at The Geysers, California Geothermal Field. *International Journal of Rock Mechanics and Mining Sciences*, 44(8), 1079–1090. doi:10.1016/j.ijrmms.2007.07.023

Orywall, P., Drüppel, K., Kuhn, D., Kohl, T., Zimmermann, M., & Eiche, E. (2017). Flow-through experiments on the interaction of sandstone with Ba-rich fluids at geothermal conditions. *Geothermal Energy*, 5(1). doi:10.1186/s40517-017-0079-7

Stark, M.A., Tom Box Jr., W., Beall, J.J., Goyal, K.P. & Pingol, A.S. (2005). The Santa Rosa -- Geysers Recharge Project, Geysers Geothermal Field, California, USA. *Proceedings World Geothermal Congress 2005*, 24-29 April 2005.

Zarrouk, S. J., & McLean, K. (2019). Geothermal well test analysis. Elsevier. doi:10.1016/c2017-0-02723-4

Zhen-Wu, B. Y., Dideriksen, K., Olsson, J., Raahauge, P. J., Stipp, S. L. S., & Oelkers, E. H. (2016). Experimental determination of barite dissolution and precipitation rates as a function of temperature and aqueous fluid composition. *Geochimica et Cosmochimica Acta*, 194, 193–210. doi:10.1016/j.gca.2016.08.041